

Does dark matter fall in the same way as standard model particles? A direct constraint of Euler’s equation with cosmological data

Nastassia Grimm,^{1,*} Camille Bonvin,^{1,†} and Isaac Tutusaus^{2,‡}

¹*Département de Physique Théorique and Center for Astroparticle Physics,
Université de Genève, Quai E. Ansermet 24, CH-1211 Geneva 4, Switzerland*

²*Institut de Recherche en Astrophysique et Planétologie (IRAP), Université de Toulouse,
CNRS, UPS, CNES, 14 Av. Edouard Belin, 31400 Toulouse, France*

(Dated: February 19, 2025)

Since dark matter particles have never been directly detected, we do not know how they move, and in particular we do not know how they fall inside gravitational potential wells. Usually it is assumed that dark matter only interacts gravitationally with itself and with particles of the standard model, and therefore that its motion is governed by Euler’s equation. In this paper, we test this assumption for the first time at cosmological scales, by combining measurements of galaxy velocities with measurements of gravitational potential wells, encoded in the Weyl potential. We find that current data are consistent with Euler’s equation at redshifts $z \in [0.3, 0.8]$, and we place constraints on the strength of a potential fifth force, which would alter the way dark matter particles fall. We find that a positive fifth force cannot exceed 7% of the gravitational interaction strength, while a negative fifth force is limited to 21%. The coming generation of surveys, including the Legacy Survey of Space and Time (LSST) of the Vera C. Rubin Observatory and the Dark Energy Spectroscopic Instrument (DESI) will drastically improve the constraints, allowing to constrain a departure from pure gravitational interaction at the level of 2%.

I. INTRODUCTION

One of the current main challenges of cosmology and of particle physics is to understand the nature and properties of dark matter. In the simplest model, dark matter is made of cold collisionless particles, which interact only gravitationally with particles of the standard model. This so-called “cold dark matter” feels gravity in the same way as standard matter, i.e., it moves along the same geodesics and obeys Euler’s equation. The existence of such cold dark matter particles is supported by cosmological observations over a wide range of scales, from the motion of stars in galaxies, and that of galaxies in clusters [1], to the large-scale structure of the Universe [2, 3] and the temperature fluctuations of the Cosmic Microwave Background (CMB) [4–6].

However, since no direct observation of such a particle has been made yet, it is legitimate to question these assumptions and explore models beyond the cold dark matter paradigm. In particular, it is important to test the validity of Euler’s equation for dark matter to determine if it falls indeed in the same way inside a gravitational potential well as standard matter. A violation of Euler’s equation for dark matter can either be gravitational, i.e., due to a breaking of the weak equivalence principle within gravity, which could couple differently to different types of matter, see e.g., [7]. Or it can be due to non-gravitational dark matter interactions, either with particles of the standard model [8–10], with a dark sector, e.g., dark radiation [11, 12] or dark energy [13–15], or with themselves [16–18]. Such interactions would directly alter the way dark matter particles fall in a gravitational potential and break the validity of Euler’s equation. In this work we focus on the second scenario: we assume that gravity is described by general relativity, which obeys the weak equivalence principle, and we search for deviations in Euler’s equation due to non-gravitational dark matter interactions.

Extensive searches for dark matter particles and their (non-gravitational) interactions have been performed via various methods: searches for dark matter collisions with particles of the standard model in Earth-based detectors, called direct search experiments, e.g., [19–22]; searches of products of dark matter decays by looking for new signals from the cosmos, called indirect search experiments, e.g., [23, 24]; and searches of dark matter particles in colliders, in particular at the Large Hadron Collider, see [25–29]. Since non-gravitational dark matter interactions (if they exist) are believed to be mediated by new particles, colliders are also searching for traces of these new particles,

* nastassia.grimm@unige.ch

† camille.bonvin@unige.ch

‡ isaac.tutusaus@irap.omp.eu

e.g., [30, 31]. In addition, non-gravitational dark matter interactions can be studied through their impact on the formation of astrophysical objects, like galaxy clusters. Self-interacting dark matter would indeed lead to a non-trivial signature in the central core of dark matter halos [32, 33] and in the alignment of galaxies [34]. In this work, we take a complementary approach, and we search for dark matter interactions at cosmological scales by probing the validity of Euler’s equation for galaxies. Since galaxies are mainly made of dark matter, by testing the relation between the velocity of galaxies and the gravitational potential Ψ , we can directly detect if dark matter particles are subject to a new force.

Cosmological surveys provide measurements of the galaxy peculiar velocities, through the so-called redshift-space distortions [35, 36]. The gravitational potential Ψ has however never been measured at cosmological scales. On the other hand, the Weyl potential, which is the sum of the time distortion Ψ and the spatial distortion Φ , $\Psi_W \equiv (\Phi + \Psi)/2$, has recently been measured using gravitational lensing data in a novel way [37]. This approach allowed for a direct measurement of Ψ_W at different redshifts. Since in general relativity, the time and spatial distortions are predicted to be the same at late time ($\Phi = \Psi$), we can use measurements of the Weyl potential $\Psi_W = \Psi$ to test the validity of Euler’s equation.

Note that if general relativity is not valid, our test will not hold, since in this case the Weyl potential Ψ_W may differ from the time distortion Ψ , and we cannot use it to test the validity of Euler’s equation. Methods have been proposed to overcome this limitation [38, 39], by measuring directly the distortion of time [40]¹, but those require the next generation of data, including DESI², the Euclid satellite³ and the Square Kilometer Array Observatory (SKAO)⁴. Hence in this study we assume that general relativity is valid, and test for the presence of non-gravitational interactions (often called fifth force) acting on dark matter in this framework.

We use recent measurements of the Weyl potential at four different redshifts [37], obtained from galaxy-galaxy lensing and galaxy clustering measurements from the first three years of Dark Energy Survey (DES) data [43], and combine them with measurements of galaxy velocities (encoded in the growth rate of structure) at 22 redshifts from various spectroscopic surveys [44–55]. With this we place constraints on the strength of the fifth force at the first four redshift bins considered for the lens galaxies in the DES Year 3 analysis [43]. We find that the parameter encoding the strength of the fifth force is compatible with zero at all redshift and can be constrained with an error ranging from 0.17 – 0.29, depending on redshift. Assuming a fifth force with constant strength over the range of observation, we constrain its amplitude to lie within –21% and 7% of the gravitational interaction strength.

We show that future surveys such as LSST⁵ and DESI will improve the constraints, allowing us to detect a departure from pure gravitational interaction at the level of 3 – 6% per redshift bin, over the range $z \in [0.51, 1.35]$. Assuming a constant strength tightens the constraints to 2%.

II. METHOD

We assume a perturbed Friedmann-Lemaître-Robertson-Walker universe, with a homogeneous and isotropic background plus perturbations, whose geometry is encoded in the metric:

$$ds^2 = a^2(\eta) \left[-(1 + 2\Psi(\mathbf{x}, \eta))d\eta^2 + (1 - 2\Phi(\mathbf{x}, \eta))\delta_{ij}dx^i dx^j \right]. \quad (1)$$

Here a is the scale factor, η denotes conformal time, and the two gravitational potentials Ψ (time distortion) and Φ (spatial distortion) encode the perturbations of the geometry. In addition, the perturbations in the matter content can be encoded into two extra fields, namely the fluctuations in the galaxy density $\delta_g = \delta\rho_g/\rho_g$ and the galaxy peculiar velocity \mathbf{V}_g . In the following we assume that the galaxy velocity is governed by the velocity of the dark matter halo $\mathbf{V}_g = \mathbf{V}_{\text{dm}}$ and we drop the subscript dm. As shown in [38], dark matter interactions generically modify Euler’s equation through two effects: an additional force encoded in the parameter $\Gamma(\eta)$ and a friction term encoded in the parameter $\theta(\eta)$:

$$V' + (1 + \theta)V - \frac{k}{7\mathcal{H}}(1 + \Gamma)\Psi = 0. \quad (2)$$

¹ Alternatively a breaking of Euler’s equation due to modified gravity can be tested through the breaking of consistency relations between $(n + 1)$ -points and n -points correlators, see [41, 42].

² <https://www.desi.lbl.gov>

³ <https://www.euclid-ec.org>

⁴ <https://www.skao.int/en>

⁵ <https://rubinobservatory.org>

In the cold dark matter scenario, $\Gamma = \theta = 0$ applies. Here V is the galaxy velocity potential in Fourier space, defined through $\mathbf{V}(\mathbf{k}, \eta) = i\mathbf{k}/kV(\mathbf{k}, \eta)$, a prime denotes derivative with respect to the logarithm of the scale factor a , and $\mathcal{H} = (da/d\eta)/a$ is the Hubble parameter in conformal time η . In many models, the parameter θ is negligible compared to the parameter Γ since it is sensitive to the time evolution of the field (scalar or vector) that governs dark matter interactions. In the quasi-static approximation the field evolves slowly and θ is negligible, see e.g., [38, 56, 57]. Hence in the following we concentrate on the dominant effect, the fifth force, and we build a method to measure the strength of the fifth force represented by Γ . Note that if instead of assuming that the velocity of galaxies is fully driven by the velocity of dark matter halos, we account for a fraction of baryons that obey Euler's equation, Γ is replaced by $x_{\text{dm}}^3 \Gamma$ where x_{dm} denotes the fraction of dark matter, see e.g. [58]. In this case, one would constrain the combination $x_{\text{dm}}^3 \Gamma$.

Galaxy surveys and weak lensing surveys cannot measure directly the velocity field $\mathbf{V}(\mathbf{k}, z)$ and the Weyl potential $\Psi_W(\mathbf{k}, z) = \Psi(\mathbf{k}, z)$ that enter into Euler's equation (2). However, the time evolution of these two fields can be measured from the galaxy correlation function and the galaxy-galaxy lensing correlation function. More precisely, spectroscopic redshift surveys like the Sloan Digital Sky Survey (SDSS)⁶ and the WiggleZ Dark Energy Survey⁷ measure the growth rate of structure as a function of redshift $\hat{f}(z) = f(z)\sigma_8(z)$, where $f(z) = d \ln \delta / d \ln a$ and $\sigma_8(z)$ denotes the amplitude of density perturbations in spheres of $8 h^{-1} \text{Mpc}$. The function $\hat{f}(z)$ governs the evolution of velocities at late time, once radiation is negligible

$$V(k, z) = \frac{\mathcal{H}(z)\hat{f}(z)}{\mathcal{H}(z_*)\hat{f}(z_*)}V(k, z_*). \quad (3)$$

To measure $\hat{f}(z)$ from galaxy surveys, one assumes that at z_* the matter power spectrum is that of a cold dark matter universe and can be tightly constrained from CMB measurements, see e.g., [59]. We will therefore keep this assumption in our analysis and assume that the fifth force is negligible at early time. This is typically the case if the fifth force is due to interactions of dark matter with dark energy, which is fully negligible at early time. If the fifth force is due to self-interacting dark matter or dark matter interacting with dark photons however, then its evolution with time is a priori unknown and it depends on the particular model. In this case, one would need to modify the matter power spectrum at z_* and redo the measurements of the growth rate $\hat{f}(z)$ for each model⁸. To keep the model-independence of our method and use current measurements of $\hat{f}(z)$, we therefore restrict our analysis to models with a negligible fifth force at z_* . Note that \hat{f} in Eq. (3) does not depend on k . This is strictly correct for cold dark matter and within general relativity.⁹ Adding a fifth force may introduce a scale-dependence of \hat{f} , however data are currently not constraining enough to test a scale-dependence [59, 62], which is why we omit it.

To test Euler's equation, in addition to \hat{f} , we need measurements of the Weyl potential. The Weyl potential governs the trajectory of light emitted by distant galaxies, and generates distortions in their observed shape. These distortions have been measured by various surveys and then used to infer the distribution of matter in the Universe, see, e.g., [43, 63]. Recently, Ref. [64] designed a novel method that uses weak lensing data to directly measure the evolution of the Weyl potential across redshift. This method was applied on DES data, combining galaxy-galaxy lensing with galaxy clustering, and provided a measurement of the function $\hat{J}(z)$ in four redshift bins [37]. This function governs the evolution of Ψ_W at late time through (see Ref. [64] for more detail)

$$\Psi_W(k, z) = \left(\frac{\mathcal{H}(z)}{\mathcal{H}(z_*)} \right)^2 \sqrt{\frac{B(k, z)}{B(k, z_*)}} \hat{J}(z) \frac{\Psi_W(k, z_*)}{\sigma_8(z_*)}. \quad (4)$$

Here $B(k, z)$ is a boost factor, encoding the non-linear evolution of matter density perturbations at small scales. The boost is introduced in the analysis to properly account for non-linearities that affect the lensing correlation function at small angular separation. In the same way as \hat{f} , the function \hat{J} is scale-independent for cold dark matter and within general relativity. As before, we neglect the possible scale-dependence introduced by a fifth force, since the data are not constraining enough to probe this. The only scale-dependence in the evolution of the Weyl potential is therefore arising through the non-linear boost $B(k, z)$. Consequently, even though \hat{f} and \hat{J} have not been measured at the same scales, since their values do not depend on the scale we can combine them to test the validity of Euler's equation in the regime of interest. Here, we concentrate on large scales, where Euler's equation is linear in V and Ψ_W .

⁶ <https://www.sdss.org>

⁷ <https://wigglez.swin.edu.au/site/forward.html>

⁸ Alternatively one can leave the matter power spectrum free and constrain it in k -bands together with the growth rate, as proposed in [39, 60].

⁹ Massive neutrinos do introduce a small scale-dependence in the growth rate f , however, in our analysis we have fixed the sum of the neutrino masses to 0.06 eV, leading to a scale-dependence which is negligible [61].

Table I. We list the first four effective redshifts of the DES MAGLIM sample along with the respective values of $\hat{J}(z)$ obtained in Ref. [37] (using CMB priors and standard scale cuts), and the values of $\hat{f}(z)$, $d \ln \hat{f}(z)/d \ln(1+z)$ and $\Gamma(z)$, with their 1σ uncertainty, obtained in this work.

z	$\hat{J}(z)$	$\hat{f}(z)$	$\frac{d \ln \hat{f}(z)}{d \ln(1+z)}$	$\Gamma(z)$
0.295	0.325 ± 0.015	0.459 ± 0.019	0.28 ± 0.17	-0.09 ± 0.17
0.467	0.333 ± 0.018	0.467 ± 0.020	0.00 ± 0.17	0.04 ± 0.17
0.626	0.387 ± 0.027	0.461 ± 0.021	-0.24 ± 0.24	-0.01 ± 0.20
0.771	0.354 ± 0.035	0.448 ± 0.024	-0.44 ± 0.31	0.16 ± 0.29

Inserting Eqs. (3) and (4) in Euler's equation (2) (setting $B = 1$ since we restrict the test to the linear regime) and using Einstein's equations and the continuity equation to relate $\Psi_W(k, z_*)$ and $V(k, z_*)$ to $\delta(k, z_*)$ we find the following relation for $\Gamma(z)$ in the linear regime

$$1 + \Gamma(z) = \frac{2\hat{f}(z)}{3\hat{J}(z)} \left(1 - \frac{d \ln \mathcal{H}(z)}{d \ln(1+z)} - \frac{d \ln \hat{f}(z)}{d \ln(1+z)} \right). \quad (5)$$

Eq. (5) is a key result of this paper. It shows that by combining measurements of \hat{J} , \hat{f} , and its derivative at a given redshift z we can *directly* measure the strength of the fifth force at that redshift. Such measurements do not require any modeling of the redshift evolution of dark matter interactions: this is directly inferred from the data. From Eq. (5), we see that these measurements require: 1) measurements of \hat{J} and \hat{f} at the same redshifts; 2) measurements of the redshift derivative of $\hat{f}(z)$; and 3) measurements of the redshift evolution of the Hubble parameter $\mathcal{H}(z)$. In the following we will assume that 3) is known from background measurements of the expansion history of the Universe, namely from luminosity distance of supernovae, baryon acoustic oscillations (BAO) and CMB measurements, and we fix it to a Λ CDM evolution. One can of course extend the method by reconstructing simultaneously $\mathcal{H}(z)$ and $\Gamma(z)$.

III. CONSTRAINTS ON EULER'S EQUATION WITH CURRENT DATA

We use 22 measurements of \hat{f} between redshifts $z = 0.001$ and $z = 1.944$, from various spectroscopic galaxy surveys [44–55]. The measurements with their uncertainties are listed in Table I of [65].¹⁰ Our aim is to infer $\Gamma(z)$ at the four DES MAGLIM effective redshifts where we have measurements of \hat{J} : $z \in \{0.295, 0.467, 0.626, 0.771\}$. We use therefore the 22 measurements of \hat{f} to reconstruct \hat{f} and its redshift derivative $d \ln \hat{f}(z)/d \ln(1+z)$ at those redshifts. We treat the four values of \hat{f} at the DES effective redshifts as free parameters and we interpolate between these parameters using cubic spline interpolation.¹¹ We then minimize the difference between the interpolated curve and the measurements of \hat{f} . The reconstructed values of \hat{f} at the four MAGLIM effective redshifts, together with the reconstruction over the whole redshift range, are plotted in the left panel of Fig. 1 and listed in Table I. The spline reconstruction also allows us to infer the redshift derivatives $d \ln \hat{f}(z)/d \ln(1+z)$ and their uncertainty at the desired redshifts. The results are plotted in the right panel of Fig. 1 and listed in Table I.

We then use these values, together with the values of \hat{J} listed in Table I, to constrain Γ following Eq. (5). The results for Γ are plotted in Fig. 2 and listed in the last column of Table I (see also the covariance matrix listed in Appendix A). We see that Γ is compatible with zero at all redshift: current data show therefore no violation of Euler's equation for dark matter. Moreover, our results put constraints on the allowed amplitude of the fifth force in each redshift bin. From Euler's equation (2), we see that gravitational interaction affects the motion of galaxies through the term $(k/\mathcal{H})\Psi$, while the impact of the fifth force is given by $\Gamma \times (k/\mathcal{H})\Psi$. This allows us to compare the strength of the fifth force with that of gravitational interaction. For example, in the first redshift bin, the fifth force is constrained to be within -26% and 8% of the gravitational interaction strength.

¹⁰ Note that the 22 values of \hat{f} used in this analysis do not include the new measurements from DESI [66]. Including these values would allow a better reconstruction in the higher redshift range $z \sim 1$ to $z \sim 2$, however, there are currently no measurements of \hat{J} available in this range. At the MAGLIM effective redshifts, including the DESI values would change the mean values only marginally, and reduce the error bars slightly by about 20%. Given this small change, we choose to not include the DESI values, as they may be correlated with some of the measurements in Table I of [65], leading to double-counting of information.

¹¹ As mentioned in [65], a spline interpolation with four free parameters is the choice that minimizes the Akaike information criterion for this data set. We also note that for this choice, i.e. a cubic spline interpolation with four knots (and applying the standard *not-a-knot* condition to fix remaining degrees of freedom), this interpolation method corresponds to a fit with one third-degree polynomial.

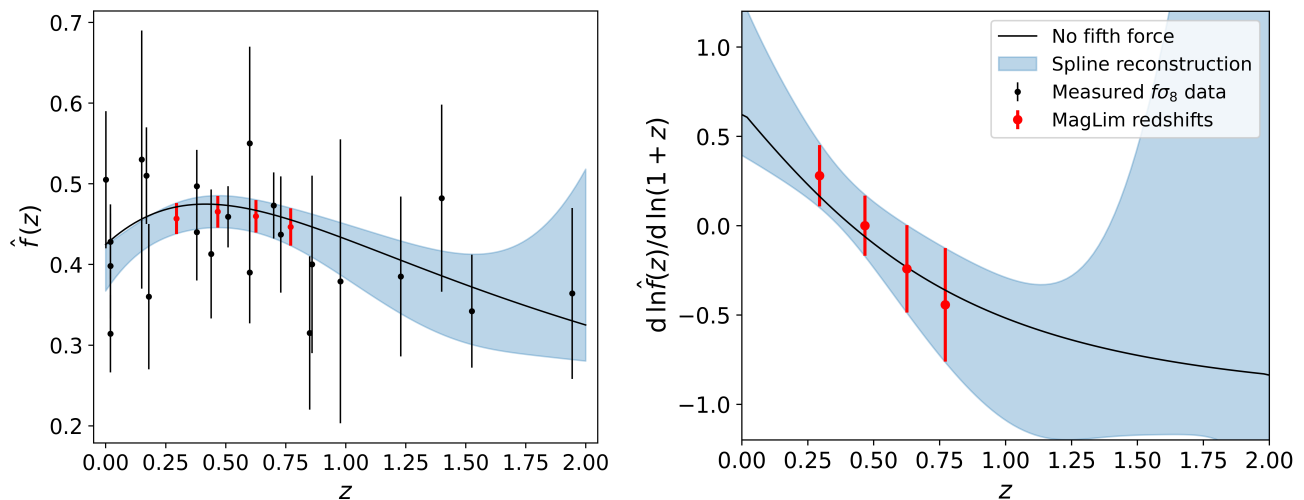


Figure 1. *Left panel:* The 22 measured data points of \hat{f} , from Table 1 of Ref. [65] (black points) and their spline reconstruction with 1σ uncertainty (blue band), leading to the values of \hat{f} at the four MAGLIM effective redshifts (red points). *Right panel:* Reconstruction of $d \ln \hat{f}(z)/d \ln(1+z)$ based on the spline interpolation of \hat{f} . For both panels, the prediction assuming no fifth force and cosmological parameters from Planck [6] is shown as well (black line), being in agreement with the reconstruction at the 1σ level.

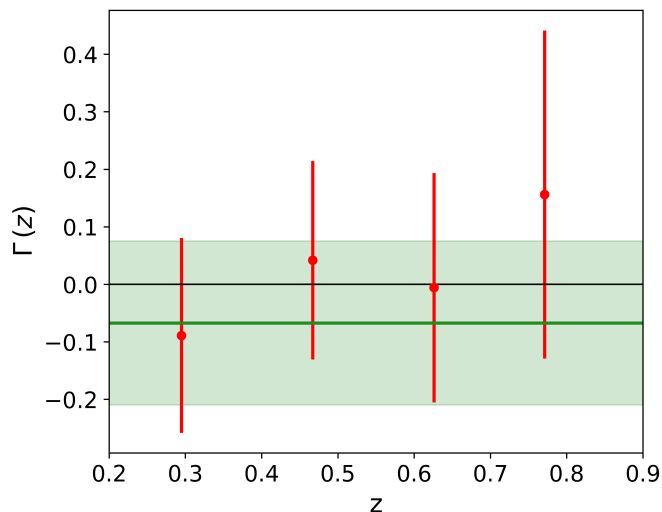


Figure 2. We show the reconstructed values (in red) of the fifth force parameter Γ together with the 1σ uncertainties at the four effective redshifts of the DES MAGLIM sample. The measurements show no deviation from Euler's equation ($\Gamma = 0$, black horizontal line). The green line with error bands shows the best-fit value and 1σ uncertainty assuming a constant value of Γ . We note that the measurements at different redshifts are correlated, as can be seen from the covariance matrix given in Appendix A.

We then assume a constant amplitude of the fifth force in the range of observation, and combine the four measurements (accounting for their covariance). We find that in this case $\Gamma = -0.07 \pm 0.14$, meaning that the amplitude of the fifth force is constrained to be within -21% and 7% of the gravitational interaction strength, see green band in Fig. 2. Finally, we examine the case where Γ is restricted to be strictly positive. This is motivated by specific models of dark matter, for example the coupling quintessence models explored in [67], where dark matter is coupled to dark energy and Γ depends on the square of the coupling strength, thus not allowing any negative fifth force. Under this restriction, we find that the fifth force cannot exceed 11% of the gravitational interaction, i.e. $\Gamma \leq 0.11$ for the 68% upper limit (and $\Gamma \leq 0.24$ for the 95% upper limit).

These constraints can be compared with the recent constraints on a dark fifth force, in a specific model with a long-

Table II. We list the first nine effective redshifts of the LSST sample along with the respective values of $\hat{J}(z)$ forecasted in Ref. [64] with 1σ uncertainties (using the pessimistic case), the values of $\hat{f}(z)$ and $d \ln \hat{f}(z)/d \ln(1+z)$ obtained at the same redshifts using the DESI forecasts [71] and spline interpolation, as well as the resulting values of $\Gamma(z)$.

z	$\hat{J}(z)$	$\hat{f}(z)$	$\frac{d \ln \hat{f}(z)}{d \ln(1+z)}$	$\Gamma(z)$
0.25	0.333 ± 0.002	0.468 ± 0.009	0.23 ± 0.19	0.00 ± 0.17
0.38	0.360 ± 0.002	0.474 ± 0.007	0.05 ± 0.10	-0.01 ± 0.09
0.51	0.378 ± 0.003	0.473 ± 0.006	-0.11 ± 0.05	0.00 ± 0.05
0.65	0.388 ± 0.003	0.466 ± 0.004	-0.26 ± 0.07	0.00 ± 0.06
0.79	0.391 ± 0.003	0.453 ± 0.003	-0.39 ± 0.07	0.01 ± 0.06
0.95	0.388 ± 0.004	0.437 ± 0.002	-0.48 ± 0.04	0.00 ± 0.03
1.13	0.380 ± 0.004	0.417 ± 0.002	-0.58 ± 0.06	0.00 ± 0.05
1.35	0.337 ± 0.004	0.392 ± 0.003	-0.69 ± 0.07	0.01 ± 0.05
1.70	0.306 ± 0.004	0.354 ± 0.008	-0.76 ± 0.39	-0.01 ± 0.26

range dark force mediated by an ultralight scalar field, derived in [68]: using CMB alone, the strength of the fifth force is constrained to be below 1.2%. Adding BAO tightens the constraints to 0.48%. These constraints are however not directly linked to a breaking of Euler’s equation, but rather driven by the background evolution of dark matter density in the model considered. More precisely, due to the additional coupling, the dark matter energy density does not decay anymore as $1/a^3$. This directly changes the redshift-distance relation in the Universe, that differs from Λ CDM predictions, leading to very tight constraints on the coupling. In practice, however, we do not know what is causing the accelerated expansion of the Universe. It could be a cosmological constant, or it could be a dynamical scalar field. Changes in distances induced by a dark fifth force are fully degenerated with changes induced by a dynamical dark energy, with equation of state parameter $w \neq -1$. In our work, we explore therefore a fully different scenario: since a signature at the level of the background cannot uniquely point to the presence of a dark fifth force, we consider that the impact of both the fifth force and any ingredient impacting the background evolution (for example the quintessence field in the case of coupled quintessence) can be encoded into an effective equation of state w_{eff} . This is the approach followed, e.g., in [67, 69]. This w_{eff} is constrained to be close to -1 by distance measurements and we therefore fix it to this value in our analysis. We then constrain the fifth force by directly looking at its impact on Euler’s equation, i.e., at the deviation it would induce on the way dark matter falls into a gravitational potential. The constraints that we obtain are an order of magnitude larger than those coming from the background evolution of dark matter density, but the advantage is that any deviations from $\Gamma = 0$ would uniquely point to the presence of a dark fifth force. No (uncoupled) dynamical dark energy model can mimic or hide such a deviation. Our approach also has the advantage that it applies to interacting dark matter models with a pure momentum exchange, that do not alter the background, see e.g. [14, 70].

Another key feature of our method is that it does not rely on any model for the fifth force evolution. We do not need to specify the form of the dark matter interaction, nor the characteristic of the field propagating the fifth force, such as the form of its potential, or its nature (scalar or vector). Our constraints are therefore model-independent. As such they can be used to constrain any model of interest, without redoing the analysis, since Γ can be related to the parameters of the model, see e.g., [38].

IV. FORECASTS WITH FUTURE SURVEYS

Our constraints rely on 22 measurements of \hat{f} from past and current spectroscopic surveys and 4 measurements of the Weyl evolution \hat{J} from photometric DES data. The coming generation of surveys, including DESI, Euclid, LSST, and SKAO, holds the potential to drastically improve on these measurements. We forecast therefore the uncertainty on the fifth force Γ , from a combination of forecast values of \hat{f} from DESI and of \hat{J} from LSST. More precisely, we use values of \hat{f} at 17 redshifts between $z = 0.15$ and $z = 1.85$ and with 1σ uncertainties as specified in Table 2.3 and Table 2.5 of Ref. [71] (we omit the lowest redshift value at $z = 0.05$, as it has a larger uncertainty and no impact on our results). These specifications assume that DESI realizes their full 14,000 square degrees of survey area, and obtains spectroscopic redshifts of more than 30 million galaxies.¹² For LSST, we use the pessimistic¹³ uncertainties forecasted

¹² The recent DESI data release utilizes 7,500 square degrees of survey area and about 4.7 million galaxies [66], and thus does not reach this potential yet. We have chosen not to include the respective values of \hat{f} in our analysis with current data, see footnote 10.

¹³ We use this choice here because it is more conservative, while having no impact on the results for Γ since the uncertainties are in any case dominated by the errors on \hat{f} and its derivative obtained from DESI data and spline reconstruction.

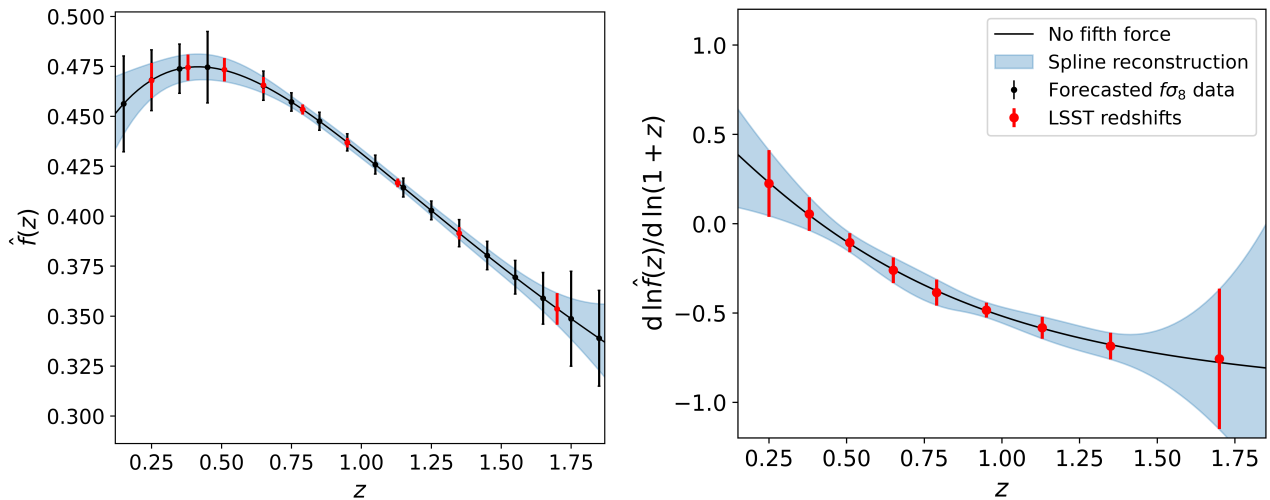


Figure 3. *Left panel:* We show 17 values for \hat{f} centered around the Λ CDM fiducial (black dots) and with 1σ uncertainties achievable by DESI covering 14,000 square degrees (see Tables 2.3 and 2.5 of [71]). We also show the spline reconstruction (blue band), leading to the values of \hat{f} at the nine effective redshifts of LSST (red dots). *Right panel:* Reconstruction of $d \ln \hat{f}(z)/d \ln(1+z)$ based on the spline interpolation of \hat{f} . For both panels, the prediction without a fifth force is shown as well (black line).

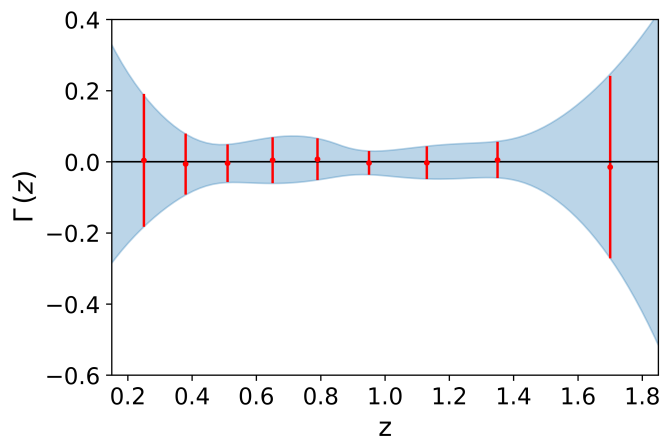


Figure 4. Using forecast values of \hat{f} from DESI [71], we show the reconstructed values (in red) of the fifth force parameter Γ together with the 1σ uncertainties at the nine effective redshifts corresponding to the LSST forecast for \hat{J} [64]. Additionally, the blue band shows a forecast over the whole redshift range when interpolating the \hat{J} data as well.

in [64] at nine redshifts between $z = 0.25$ and $z = 1.7$ (omitting the forecast at $z = 2.1$ since this is well beyond the range where \hat{f} data from DESI will be available), see the first two columns of Table II. We center the values of \hat{f} and \hat{J} around their prediction assuming no fifth force and cosmological parameters from Planck [6]. For \hat{J} , we account for the covariance between redshift bins, which is non-zero due to the non-negligible overlap of the photometric redshift bins (see Fig. 1 of [64]). For DESI, we neglect the covariance between the bins, which is expected to be small due to the sharp edges of the bins in spectroscopic samples. This assumption can be tested once data from the completed DESI survey are available, and if needed the covariance can easily be included.

On the left panel of Fig. 3, we plot the forecast data for \hat{f} as well as their interpolation over the whole redshift range, $z \in [0.15, 1.85]$, again using spline interpolation.¹⁴ We have tested that spline interpolation with four knots

¹⁴ As an alternative interpolation method, we have as well considered Gaussian processes, as recent research has suggested that they may

is not sufficient to describe this future data set well, leading to a deviation from the fiducial value of zero in the reconstruction of $\Gamma(z)$. Thus, we are using five knots, with the central one located at $z = 0.86$ as we find that this placement minimizes the Akaike information criterion.¹⁵ On the right panel, we show the resulting reconstruction of $d \ln \hat{f}(z)/d \ln(1+z)$. The values of these quantities at the LSST effective redshifts, where future measurements of \hat{J} will be available, are indicated in red in the figure and listed in the third and fourth column of Table II. Finally, in Fig. 4, we show (in red) the results for Γ at the LSST redshifts. As we have nine values of \hat{J} with very high precision, we can perform a spline interpolation between these values, and therefore obtain a reconstruction (in blue) of Γ along the whole redshift range, $z \in [0.15, 1.85]$. The constraints at the LSST redshifts are also listed in the last column of Table II. We see that the constraints are significantly tighter than current ones. We also note that the mean values for Γ are, as a result of the spline interpolation, not always exactly equal to the fiducial value of zero. However, the fiducial value is always well contained within the 1σ error bars, meaning that the interpolation method does not lead to any false imprints of new physics. In particular, over the range $z \in [0.51, 1.35]$, we find that DESI combined with LSST will allow to detect a departure from pure gravitational interaction at the level of 3 – 6% per redshift bin. Assuming a constant strength of the fifth force and applying the results for Γ at the LSST redshifts (including their covariance), we find that the combination of DESI and LSST data will allow to constrain a fifth force with amplitude down to 2% of the gravitational interaction strength.

In our analysis and forecasts, we have assumed that general relativity is valid at cosmological scales. In this scenario, any deviation in Euler’s equation would be due to non-gravitational dark matter interactions. If general relativity is not valid however, Euler’s equation could be violated by the new degree of freedom mediating gravity, that could break the equivalence principle between standard matter and dark matter, see, e.g., [7]. Alternatively, in models beyond general relativity, the time distortion and the spatial distortion can be different [73, 74], leading to an apparent breaking of Euler’s equation due to the fact that we used the Weyl potential Ψ_W instead of the time distortion Ψ . To distinguish between these scenarios, one would need to measure directly the time distortion Ψ . As shown in [40], this will be possible with future surveys like DESI, Euclid, and the SKAO, by looking at the impact of gravitational redshift on the distribution of galaxies. Combining these new measurements of Ψ with that of the Weyl potential and of the galaxy velocities will allow us to distinguish between a non-gravitational interaction that would affect only Euler’s equation, a modification of gravity that would generate a difference between Ψ and Ψ_W [58, 67], and a modified gravity model that would break the weak equivalence principle and modify both Euler’s equation and the relation between Ψ and Ψ_W .

V. CONCLUSION

In this paper we have performed the first direct test of the validity of Euler’s equation for dark matter at cosmological scales. We have combined measurements of galaxy peculiar velocities with measurements of the Weyl potential, to place constraints on the existence of a fifth force that would alter the way dark matter falls inside a gravitational potential. We have found that current data do not favor the existence of such a fifth force, and we have placed constraints on the strength of interaction in four redshift bins. Moreover, assuming that the strength of the fifth force is constant over our range of observation, we have found that a positive fifth force cannot exceed 7% of the gravitational interaction strength, while a negative fifth force is constrained to be less than 21% of the strength. Future data will improve the precision and allow to detect departures from pure gravitational interaction at the level of 3 – 6% per redshift bin, and at 2% assuming a constant amplitude.

In our analysis we have let the parameter encoding the strength of the fifth force take any sign. In specific models of dark matter interactions, the sign is determined by the physical impact of the interaction. For example, in some models of dark energy coupled with dark matter, the fifth force is positive (proportional to the square of the coupling strength) and enhances the clustering of dark matter [67]. On the other hand, if dark matter interacts with dark radiation, it can lead to a force that effectively reduces the clustering with respect to pure gravitational interaction [75], which can be represented by a negative Γ . Similarly, specific models of dark matter coupled to dark energy with a pure momentum exchange also lead to an effective decrease of dark matter clustering [70].¹⁶ Finally, in the case where gravity is modified and the weak equivalence principle is broken, dark matter can feel a larger or smaller interaction than baryons, leading to any sign for Γ .

be applicable to next-generation large-scale structure data [72]. However, for the DESI specifications applied in this work, we have found that Gaussian processes lead to a biased reconstruction of \hat{f} and its derivative, showing a deviation from the fiducial model. Thus, we have chosen to show results for spline interpolation only.

¹⁵ Applying spline interpolation with five knots, and enforcing the *not-a-knot* boundary condition, results in two third-degree polynomials connected at the central knot. The values of the remaining knots serve to fix the degrees of freedom of the polynomials, but the precise placements of these knots do not influence the reconstruction.

¹⁶ Note that not all interacting dark matter models can be described by Eq. (2) with a free parameter Γ . However, even more complicated modifications can be absorbed in an effective Γ , that has no physical meaning (and can depend on ratio of perturbations) but effectively captures a deviation in Euler’s equation.

A remarkable characteristic of our analysis is that it does not require to specify the type of dark matter interaction responsible for the breaking of Euler's equation, nor its time evolution. Since galaxy velocities as well as the Weyl potential can be measured at different moments of the history of the Universe, they can be used to test Euler's equation redshift bin by redshift bin. This is particularly interesting in the case where dark matter would interact with dark energy, whose impact becomes more and more relevant at low redshift. In such a scenario, one could expect a fifth force growing with time. Future surveys, that will provide measurements of the growth rate \hat{f} and the Weyl potential \hat{J} in a larger number of bins, and over a larger redshift range, will make optimal use of this characteristic, allowing a refined reconstruction of the evolution of the fifth force. Finally, while not having been a subject of this work, we note that the high precision of future surveys may allow us to probe a scale-dependence of \hat{f} as well as \hat{J} . Our method to constrain the fifth force by combining these quantities could be easily extended to such cases, taking the binning in scale in addition to the binning in redshift into account. Thus, future surveys hold the potential to provide precise results on the existence of a fifth force, as well as on its scale- and redshift-behavior.

ACKNOWLEDGMENTS

N.G. and C.B. acknowledge support from the European Research Council (ERC) under the European Union's Horizon 2020 research and innovation program (grant agreement No. 863929; project title "Testing the law of gravity with novel large-scale structure observables").

Appendix A: Covariance matrix for the parameter Γ from current data

Below, we list the covariance matrix for the four values of Γ obtained from current data, as described in Section III:

$$\text{Cov}(\Gamma) = \begin{pmatrix} 0.0282 & 0.0173 & 0.0081 & 0.0026 \\ 0.0173 & 0.0294 & 0.0282 & 0.0328 \\ 0.0081 & 0.0282 & 0.0400 & 0.0478 \\ 0.0026 & 0.0328 & 0.0478 & 0.0748 \end{pmatrix}. \quad (\text{A1})$$

-
- [1] Bertone, G. & Hooper, D. History of dark matter. *Rev. Mod. Phys.* **90**, 045002 (2018). 1605.04909.
 - [2] Blumenthal, G. R., Faber, S. M., Primack, J. R. & Rees, M. J. Formation of Galaxies and Large Scale Structure with Cold Dark Matter. *Nature* **311**, 517–525 (1984).
 - [3] Davis, M., Efstathiou, G., Frenk, C. S. & White, S. D. M. The Evolution of Large Scale Structure in a Universe Dominated by Cold Dark Matter. *Astrophys. J.* **292**, 371–394 (1985).
 - [4] Peebles, P. J. E. Large scale background temperature and mass fluctuations due to scale invariant primeval perturbations. *Astrophys. J. Lett.* **263**, L1–L5 (1982).
 - [5] Hinshaw, G. *et al.* Nine-year Wilkinson Microwave Anisotropy Probe (WMAP) Observations: Cosmological Parameter Results. *Astrophys. J. Supp. Series* **208**, 19 (2013). 1212.5226.
 - [6] Aghanim, N. *et al.* Planck 2018 results. VI. Cosmological parameters. *Astron. Astrophys.* **641**, A6 (2020). [Erratum: *Astron. Astrophys.* 652, C4 (2021)], 1807.06209.
 - [7] Gleyzes, J., Langlois, D., Mancarella, M. & Vernizzi, F. Effective Theory of Interacting Dark Energy. *JCAP* **08**, 054 (2015). 1504.05481.
 - [8] Barkana, R. Possible interaction between baryons and dark-matter particles revealed by the first stars. *Nature* **555**, 71–74 (2018). 1803.06698.
 - [9] Schewtschenko, J. A. *et al.* Dark matter–radiation interactions: the structure of Milky Way satellite galaxies. *Mon. Not. Roy. Astron. Soc.* **461**, 2282–2287 (2016). 1512.06774.
 - [10] Diacomis, J. A. D. & Wong, Y. Y. Y. On the prior dependence of cosmological constraints on some dark matter interactions. *JCAP* **05**, 025 (2019). 1811.11408.
 - [11] Diamanti, R., Giusarma, E., Mena, O., Archidiacono, M. & Melchiorri, A. Dark Radiation and interacting scenarios. *Phys. Rev. D* **87**, 063509 (2013). 1212.6007.
 - [12] Buen-Abad, M. A., Marques-Tavares, G. & Schmaltz, M. Non-Abelian dark matter and dark radiation. *Phys. Rev. D* **92**, 023531 (2015). 1505.03542.
 - [13] Pettorino, V., Amendola, L., Baccigalupi, C. & Quercellini, C. Constraints on coupled dark energy using CMB data from WMAP and south pole telescope. *Phys. Rev. D* **86** (2012). 1207.3293.
 - [14] Pourtsidou, A., Skordis, C. & Copeland, E. J. Models of dark matter coupled to dark energy. *Phys. Rev. D* **88**, 083505 (2013). 1307.0458.

- [15] Costa, A. A., Olivari, L. C. & Abdalla, E. Quintessence with Yukawa Interaction. *Phys. Rev. D* **92**, 103501 (2015). 1411.3660.
- [16] Spergel, D. N. & Steinhardt, P. J. Observational evidence for selfinteracting cold dark matter. *Phys. Rev. Lett.* **84**, 3760–3763 (2000). astro-ph/9909386.
- [17] Archidiacono, M., Castorina, E., Redigolo, D. & Salvioni, E. Unveiling dark fifth forces with linear cosmology. *JCAP* **10**, 074 (2022). 2204.08484.
- [18] Tulin, S. & Yu, H.-B. Dark Matter Self-interactions and Small Scale Structure. *Phys. Rept.* **730**, 1–57 (2018). 1705.02358.
- [19] Behnke, E. *et al.* Final Results of the PICASSO Dark Matter Search Experiment. *Astropart. Phys.* **90**, 85–92 (2017). 1611.01499.
- [20] Abdelhameed, A. H. *et al.* First results from the CRESST-III low-mass dark matter program. *Phys. Rev. D* **100**, 102002 (2019). 1904.00498.
- [21] Agnes, P. *et al.* Search for low-mass dark matter WIMPs with 12 ton-day exposure of DarkSide-50. *Phys. Rev. D* **107**, 063001 (2023). 2207.11966.
- [22] Aalbers, J. *et al.* First Dark Matter Search Results from the LUX-ZEPLIN (LZ) Experiment. *Phys. Rev. Lett.* **131**, 041002 (2023). 2207.03764.
- [23] Gaskins, J. M. A review of indirect searches for particle dark matter. *Contemp. Phys.* **57**, 496–525 (2016). 1604.00014.
- [24] Conrad, J. & Reimer, O. Indirect dark matter searches in gamma and cosmic rays. *Nature Phys.* **13**, 224–231 (2017). 1705.11165.
- [25] Rodríguez, A. B. *et al.* Prospects on searches for baryonic Dark Matter produced in b-hadron decays at LHCb. *Eur. Phys. J. C* **81**, 964 (2021). 2106.12870.
- [26] Hayrapetyan, A. *et al.* Dark sector searches with the CMS experiment (2024). 2405.13778.
- [27] Aad, G. *et al.* The quest to discover supersymmetry at the ATLAS experiment (2024). 2403.02455.
- [28] Aad, G. *et al.* Exploration at the high-energy frontier: ATLAS Run 2 searches investigating the exotic jungle beyond the Standard Model (2024). 2403.09292.
- [29] Ariga, A. *et al.* FASER’s physics reach for long-lived particles. *Phys. Rev. D* **99**, 095011 (2019). 1811.12522.
- [30] Aaij, R. *et al.* Search for $A' \rightarrow \mu^+ \mu^-$ decays. *Phys. Rev. Lett.* **124**, 041801 (2020). URL <https://link.aps.org/doi/10.1103/PhysRevLett.124.041801>.
- [31] Aad, G. *et al.* ATLAS searches for additional scalars and exotic Higgs boson decays with the LHC Run 2 dataset (2024). 2405.04914.
- [32] Robertson, A. *et al.* Observable tests of self-interacting dark matter in galaxy clusters: cosmological simulations with SIDM and baryons. *Mon. Not. Roy. Astron. Soc.* **488**, 3646–3662 (2019). 1810.05649.
- [33] Eckert, D. *et al.* Constraints on dark matter self-interaction from the internal density profiles of X-COP galaxy clusters. *Astron. Astrophys.* **666**, A41 (2022). 2205.01123.
- [34] Harvey, D., Chisari, N. E., Robertson, A. & McCarthy, I. G. The impact of self-interacting dark matter on the intrinsic alignments of galaxies. *Mon. Not. Roy. Astron. Soc.* **506**, 441–451 (2021). 2104.02093.
- [35] Kaiser, N. Clustering in real space and in redshift space. *Mon. Not. Roy. Astron. Soc.* **227**, 1–27 (1987).
- [36] Hamilton, A. J. S. *Linear Redshift Distortions: A Review*, 185–275 (Springer Netherlands, Dordrecht, 1998). URL https://doi.org/10.1007/978-94-011-4960-0_17. astro-ph/9708102.
- [37] Tutusaus, I., Bonvin, C. & Grimm, N. Measurement of the Weyl potential evolution from the first three years of dark energy survey data. *Nature Commun.* **15**, 9295 (2024). 2312.06434.
- [38] Bonvin, C. & Fleury, P. Testing the equivalence principle on cosmological scales. *JCAP* **05**, 061 (2018). 1803.02771.
- [39] Castello, S., Zheng, Z., Bonvin, C. & Amendola, L. Testing the equivalence principle across the Universe: a model-independent approach with galaxy multi-tracing (2024). 2412.08627.
- [40] Sobral-Blanco, D. & Bonvin, C. Measuring the distortion of time with relativistic effects in large-scale structure. *Mon. Not. Roy. Astron. Soc.* **519**, L39–L44 (2022). 2205.02567.
- [41] Kehagias, A., Noreña, J., Perrier, H. & Riotto, A. Consequences of Symmetries and Consistency Relations in the Large-Scale Structure of the Universe for Non-local bias and Modified Gravity. *Nucl. Phys. B* **883**, 83–106 (2014). 1311.0786.
- [42] Creminelli, P., Gleyzes, J., Hui, L., Simonović, M. & Vernizzi, F. Single-Field Consistency Relations of Large Scale Structure. Part III: Test of the Equivalence Principle. *JCAP* **06**, 009 (2014). 1312.6074.
- [43] Abbott, T. M. C. *et al.* Dark Energy Survey Year 3 results: Cosmological constraints from galaxy clustering and weak lensing. *Phys. Rev. D* **105**, 023520 (2022). 2105.13549.
- [44] Howlett, C. *et al.* 2MTF – VI. Measuring the velocity power spectrum. *Mon. Not. Roy. Astron. Soc.* **471**, 3135–3151 (2017). 1706.05130.
- [45] Huterer, D., Shafer, D., Scolnic, D. & Schmidt, F. Testing Λ CDM at the lowest redshifts with SN Ia and galaxy velocities. *JCAP* **05**, 015 (2017). 1611.09862.
- [46] Hudson, M. J. & Turnbull, S. J. The growth rate of cosmic structure from peculiar velocities at low and high redshifts. *Astrophys. J. Lett.* **751**, L30 (2013). 1203.4814.
- [47] Turnbull, S. J. *et al.* Cosmic flows in the nearby universe from Type Ia Supernovae. *Mon. Not. Roy. Astron. Soc.* **420**, 447–454 (2012). 1111.0631.
- [48] Davis, M. *et al.* Local Gravity versus Local Velocity: Solutions for β and nonlinear bias. *Mon. Not. Roy. Astron. Soc.* **413**, 2906 (2011). 1011.3114.
- [49] Song, Y.-S. & Percival, W. J. Reconstructing the history of structure formation using Redshift Distortions. *JCAP* **10**, 004 (2009). 0807.0810.

- [50] Blake, C. *et al.* Galaxy And Mass Assembly (GAMA): improved cosmic growth measurements using multiple tracers of large-scale structure. *Mon. Not. Roy. Astron. Soc.* **436**, 3089 (2013). 1309.5556.
- [51] Alam, S. *et al.* Completed SDSS-IV extended Baryon Oscillation Spectroscopic Survey: Cosmological implications from two decades of spectroscopic surveys at the Apache Point Observatory. *Phys. Rev. D* **103**, 083533 (2021). 2007.08991.
- [52] Blake, C. *et al.* The WiggleZ Dark Energy Survey: Joint measurements of the expansion and growth history at $z < 1$. *Mon. Not. Roy. Astron. Soc.* **425**, 405–414 (2012). 1204.3674.
- [53] Pezzotta, A. *et al.* The VIMOS Public Extragalactic Redshift Survey (VIPERS): The growth of structure at $0.5 < z < 1.2$ from redshift-space distortions in the clustering of the PDR-2 final sample. *Astron. Astrophys.* **604**, A33 (2017). 1612.05645.
- [54] Okumura, T. *et al.* The Subaru FMOS galaxy redshift survey (FastSound). IV. New constraint on gravity theory from redshift space distortions at $z \sim 1.4$. *Publ. Astron. Soc. Jap.* **68**, 38 (2016). 1511.08083.
- [55] Zhao, G.-B. *et al.* The clustering of the SDSS-IV extended Baryon Oscillation Spectroscopic Survey DR14 quasar sample: a tomographic measurement of cosmic structure growth and expansion rate based on optimal redshift weights. *Mon. Not. Roy. Astron. Soc.* **482**, 3497–3513 (2019). 1801.03043.
- [56] Khoury, J. & Weltman, A. Chameleon fields: Awaiting surprises for tests of gravity in space. *Phys. Rev. Lett.* **93**, 171104 (2004). astro-ph/0309300.
- [57] Hinterbichler, K. & Khoury, J. Symmetron Fields: Screening Long-Range Forces Through Local Symmetry Restoration. *Phys. Rev. Lett.* **104**, 231301 (2010). 1001.4525.
- [58] Bonvin, C. & Pogosian, L. Modified Einstein versus Modified Euler for Dark Matter. *Nature Astron.* **7**, 1127–1134 (2023). 2209.03614.
- [59] Satpathy, S. *et al.* The clustering of galaxies in the completed SDSS-III Baryon Oscillation Spectroscopic Survey: On the measurement of growth rate using galaxy correlation functions. *Mon. Not. Roy. Astron. Soc.* **469**, 1369–1382 (2017). 1607.03148.
- [60] Schirra, A. P., Quartin, M. & Amendola, L. A model-independent measurement of the expansion and growth rates from BOSS using the FreePower method (2024). 2406.15347.
- [61] Blanchard, A. *et al.* Euclid preparation: VII. Forecast validation for Euclid cosmological probes. *Astron. Astrophys.* **642**, A191 (2020). 1910.09273.
- [62] Amendola, L., Pietroni, M. & Quartin, M. Fisher matrix for the one-loop galaxy power spectrum: measuring expansion and growth rates without assuming a cosmological model. *JCAP* **11**, 023 (2022). 2205.00569.
- [63] Asgari, M. *et al.* KiDS-1000 Cosmology: Cosmic shear constraints and comparison between two point statistics. *Astron. Astrophys.* **645**, A104 (2021). 2007.15633.
- [64] Tutusaus, I., Sobral-Blanco, D. & Bonvin, C. Combining gravitational lensing and gravitational redshift to measure the anisotropic stress with future galaxy surveys. *Phys. Rev. D* **107** (2023). 2209.08987.
- [65] Grimm, N., Bonvin, C. & Tutusaus, I. Testing General Relativity through the EG Statistic Using the Weyl Potential and Galaxy Velocities. *Phys. Rev. Lett.* **133**, 211004 (2024). 2403.13709.
- [66] Adame, A. G. *et al.* DESI 2024 V: Full-Shape Galaxy Clustering from Galaxies and Quasars (2024). 2411.12021.
- [67] Castello, S., Wang, Z., Dam, L., Bonvin, C. & Pogosian, L. Disentangling modified gravity from a dark force with gravitational redshift. *Phys. Rev. D* **110**, 103523 (2024). 2404.09379.
- [68] Bottaro, S., Castorina, E., Costa, M., Redigolo, D. & Salvioni, E. Unveiling dark forces with the Large Scale Structure of the Universe. *Phys. Rev. Lett.* **132**, 201002 (2024). 2309.11496.
- [69] Wang, Z., Mirpoorian, S. H., Pogosian, L., Silvestri, A. & Zhao, G.-B. New MGCAMB tests of gravity with CosmoMC and Cobaya. *JCAP* **08**, 038 (2023). 2305.05667.
- [70] Chamings, F. N., Avgoustidis, A., Copeland, E. J., Green, A. M. & Pourtsidou, A. Understanding the suppression of structure formation from dark matter-dark energy momentum coupling. *Phys. Rev. D* **101**, 043531 (2020). 1912.09858.
- [71] Aghamousa, A. *et al.* The DESI Experiment Part I: Science, Targeting, and Survey Design (2016). 1611.00036.
- [72] Perenon, L. *et al.* Multi-tasking the growth of cosmological structures. *Phys. Dark Univ.* **34**, 100898 (2021). 2105.01613.
- [73] Amendola, L., Kunz, M. & Sapone, D. Measuring the dark side (with weak lensing). *JCAP* **0804**, 013 (2008). 0704.2421.
- [74] Daniel, S. F., Caldwell, R. R., Cooray, A. & Melchiorri, A. Large Scale Structure as a Probe of Gravitational Slip. *Phys. Rev. D* **77**, 103513 (2008). 0802.1068.
- [75] Archidiacono, M. *et al.* Constraining Dark Matter-Dark Radiation interactions with CMB, BAO, and Lyman- α . *JCAP* **10**, 055 (2019). 1907.01496.